ACS APPLIED POLYMER MATERIALS

pubs.acs.org/acsapm Article

Thermal Annealing of High *cis*-1,4-Polybutadiene/Octadecyl Acrylate Blends as a One-Step Process for Fabricating Shape Memory Polymers

Sayan Basak, Juan Camilo Marin Angel, and Kevin A. Cavicchi*

Cite This: https://doi.org/10.1021/acsapm.3c00319 Read Online

ACCESS | Metrics & More | Article Recommendations | Supporting Information

ABSTRACT: Blending molecular crystals with a cross-linkable elastomer is an inexpensive, formulation- and processing-friendly route to develop shape memory polymers (SMPs). In this work, a shape memory material consisting of thermally cross-linked, octadecyl acrylate (ODA)-grafted polybutadiene (PB) and free octadecyl acrylate was prepared. High-temperature (175 °C) annealing of a melt-processable blend of PB and ODA results in the ene grafting of a portion of the ODA onto the PB chains producing a side-chain crystalline polymer, while simultaneous cross-linking of the PB produces a cross-linked network. At ODA loadings of 0.66 ODA molecules:PB repeat unit (80 wt % ODA), materials with high shape fixity (>99%) and recovery (>99%) were prepared. Higher shape recovery was measured compared to previously reported peroxide cross-linked PB/ODA blends. Limited blooming of the free ODA was found on stored samples and during shape memory cycling, an improvement compared to other elastomer small molecule blends. These results are discussed in terms of the synthesis, structure, and physical properties of this blend system.

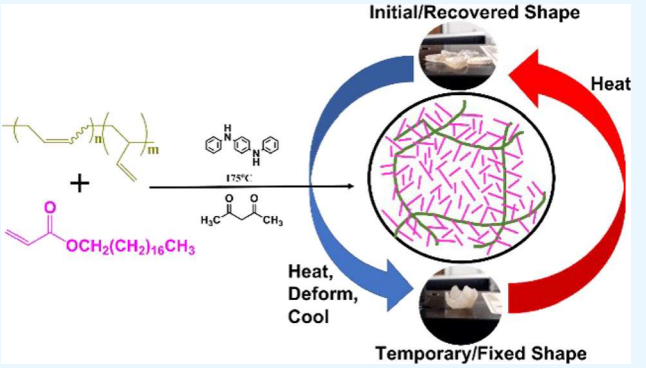

KEYWORDS: *ene reaction, n-octadecyl acrylate, polybutadiene, polymer blends, shape memory polymers*

1. INTRODUCTION

Shape memory polymers (SMPs) are an important class of stimuli-responsive materials.[1−4] A common, everyday example is heat shrink film prepared by crystallizing cross-linked low-density polyethylene in a stretched state.[5] In general, the programming of a temporary shape and stimuli-driven recovery of an initial shape are enabled by a judicious combination of the elastic properties of cross-linked polymer networks with the reversible chain immobilization of thermoplastic materials. The shape memory effect has a long history in polymer materials, being first reported in polymethyl methacrylate for use in dental molds,[6] and continues to be an active area of research due to the utility of programmable shape change in materials ranging from commodity packaging[7] to advanced biomedical devices.[8,9]

A polymer material with a tunable shape memory effect typically requires a multicomponent material to incorporate both thermoplastic and elastic elements. This may be done synthetically by preparing copolymers (e.g., polyurethane block copolymers)[10] or physically by blending.[11] This blending approach allows the synthesis of different components to be decoupled and potentially provides a wider formulation space. Small molecules, such as waxes,[12] fatty acids,[13] and hindered phenols,[14] have been mixed with different elastomers to generate reversible solid networks (i.e., thermoplastic behavior) necessary for the function of SMPs. These small molecule additives offer the advantage of good mixing and dispersion due to their higher miscibility and diffusivity compared to polymer analogues. A potential drawback is the lack of covalent attachment to the polymer network, which can lead to the blooming or leaching of the small molecule during storage and shape memory cycling of the material.[15,16] However, this effect can be mitigated through specific interactions between the polymer and additive, such as in blends of sulfonated EPDM (sulfonated poly{ethylene-*r*-propylene-*r*-(5-ethylidene-2-norbornene)} ionomer) and neutralized fatty acids.[17] Nevertheless, a recent approach to capitalize on the positive attributes of polymer/small molecule blends in fabricating SMPs is to use a monomer as the small molecule additive, which after blending can be polymerized making it more

Received: February 17, 2023
Accepted: May 24, 2023

Scheme 1. Chemical Structures of the Materials Used in This Work

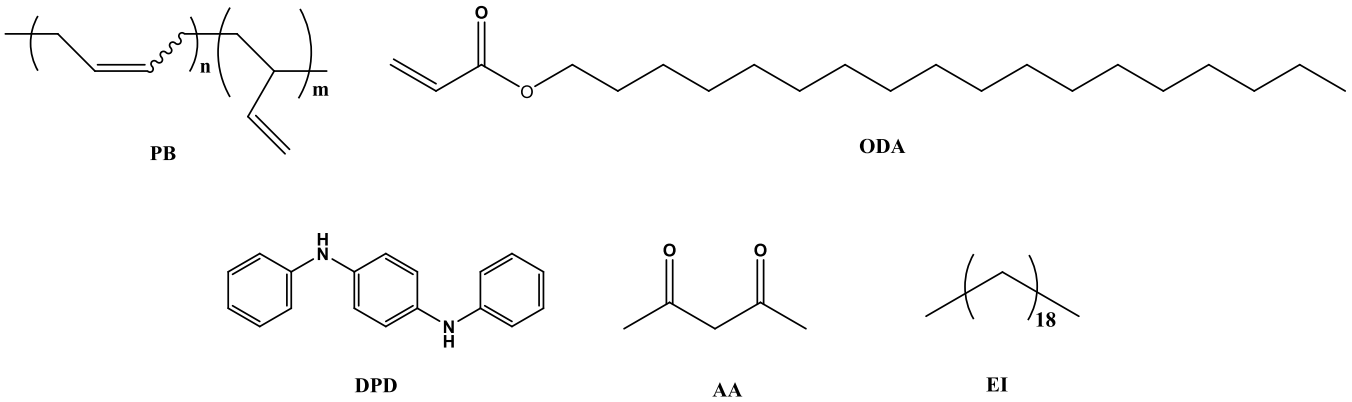

difficult to remove from the SMP. Both Cavicchi and coworkers and Okay and coworkers have investigated the free radical polymerization of octadecyl acrylate (ODA) and simultaneous cross-linking of unsaturated elastomer precursor polymers to produce SMPs by thermal (Cavicchi)[18,19] and photo-polymerization (Okay).[20−22] Poly(octadecyl acrylate) (PODA) is a side-chain crystalline polymer that produces thermoplastic domains in cross-linked materials resulting in excellent shape memory properties. In both cases, while PODA serves as the network that promotes shape fixing, the cross-linked elastomer drives the material to revert to its original shape.

This work presents an alternative approach to fabricating an SMP using a blend of ODA and high-*cis*-1,4-polybutadiene (PB) to fabricate a material more similar to previously studied polymer/molecular crystal blends. Here, the ODA is used as a grafting agent where grafting of a portion of ODA onto PB and cross-linking of the PB occurs simultaneously in thermally annealed samples. This is done without any peroxide initiator and therefore avoids the potential hazards of working with peroxide-containing materials as examined in our previous work.[18,19] This present work follows the previous reports of Luchtenberg et al. who showed the grafting of ODA to PB by an Alder-ene reaction.[23] They observed no gelation when they heated PB (M_n = 1700 g/mol, 75 mol % 1,4-*cis*, 24 mol % 1,4-*trans*, and 1 mol % vinyl) with ODA in the presence of *N*,*N*-diphenyl-*p*-phenylenediamine, and acetylacetone in a dark reaction vessel under a nitrogen atmosphere at 180 °C for 25 h. However, in this current study, a higher MW PB (M_n = 234,322 g/mol) was used where gelation occurs due to a thermally driven cross-linking reaction along with simultaneous ODA grafting of PB, resulting in a cross-linked graft network mixed with ODA crystals capable of exhibiting shape memory properties. The shape memory properties (especially shape recovery) of this grafted elastomeric network improved compared to the previous peroxide cured ODA/PB blend and is attributed to the more complete incorporation of PB into the elastic network, preventing the presence of viscoelastic material that can stress-relax in the programmed or deformed state limiting the shape recovery. Under the reaction conditions, the grafting was not 100% efficient leaving unreacted ODA in the final SMP. However, blooming was not observed in the stored materials, which is speculated to be due to the good compatibility of the graft copolymer with the ODA and cross-linking in a stress-free state. This was investigated by comparing these materials to analogous annealed blends of PB and eicosane, where cross-linking occurs, but grafting to form side-chain crystalline polymer does not occur. In the case of PB/eicosane blends, the blooming of the small molecule was observed over time.

This paper demonstrates the proof of concept of fabricating SMPs from blends of an elastomer and a functional additive that acts as both a graftable side-chain crystalline unit and a crystalline filler. While the first section of the paper investigates the chemistry of the PB intermolecular cross-linking along with the grafting of the ODA onto the PB, the second section focuses on the physical, mechanical, and structural properties of these graft polymers. In the third section, the quantitative shape memory properties are discussed and contrasted with our previously studied peroxide cured system and more generally with other reported elastomer/polyODA systems. Overall, this study presents a melt-processable formulation of a PB-ODA mixture compatible with common molding techniques to produce shape-memory polymers with excellent shape fixity (>99%) and shape recovery (>99%).

2. EXPERIMENTAL SECTION

2.1. Materials. Polybutadiene (*EC140*) was obtained from Bridgestone with molecular characteristics of M_w = 455,000 g/mol, M_n = 234,322 g/mol, and $Đ$ = 1.94 determined by gel permeation chromatography calibrated with polystyrene standards. Proton NMR analysis using the formula given in ref 24 gave a microstructure of 99.45% 1,4 content. Octadecyl acrylate (ODA) >97% pure, stabilized with 4-methoxyphenol (TCI chemicals), *N*,*N*′-diphenyl-*p*-phenylenediamine (DPD) (Sigma-Aldrich), acetylacetone (AA) (TCI Chemicals), *n*-eicosane (EI) (99%, Alfa Aesar), hexane (98.5%, Fisher Scientific Co.), toluene (99.9%, Fisher Scientific Co.), chloroform-*d* (99.9%, Fisher Scientific Co.), tetrahydrofuran (HiPerSolv CHROMANORM, VWR Chemicals), and tetrahydrofuran (99%, Sigma-Aldrich) were used as received. Scheme 1 shows the structure of these materials.

2.2. Sample Preparation. Solvent cast samples were prepared by dissolving PB (0.4−2 g), ODA (0−1.6 g) or eicosane (0.56−1.6 g), DPD (0.05 wt % of the total weight of the sample), and AA (0.01 wt % of the total weight of the sample) in 20 mL of hexane for 24 h. DPD and AA were used as an inhibitor package based on the previous work on the grafting of ODA to PB.[23,25] Each solution was poured into a 70 mm diameter Teflon dish, and the solvent was evaporated after covering the dish with perforated aluminum foil to facilitate slow solvent evaporation and prevent the formation of any bubbles on the surface of the cast film. The cast film was then placed in a circular spacer (1 mm thick, 60 mm inner diameter, and 75 mm outer diameter) and pressed with thermostated caged platens (Low Temp Plate LT2) using a compression molder (Dake) at 175 °C, under an applied load of 40 kg/cm^2 for 4 h. The blends were referred to as PB-

https://doi.org/10.1021/acsapm.3c00319
ACS Appl. Polym. Mater. XXXX, XXX, XXX−XXX

*x*ODA or PB-*x*EI, where *x* was the moles of ODA or EI per moles of PB repeat unit.

Samples with higher ODA loadings (PB-10.07ODA, PB-13.7ODA, PB-20.6ODA, PB-27.3ODA, PB-41.4ODA) were prepared by weighing out PB and ODA along with DPD (0.05 wt % of the total weight of the sample) and AA (0.01 wt % of the total weight of the sample) in 20 mL silicone septa-capped vials and heated in a thermostated aluminum reaction block at 60 °C for 24 h. The vials were shaken periodically to ensure the formation of a PB/ODA homogeneous mixture. Once mixed, these samples were sparged with nitrogen gas for 15 min at 60 °C to degas the samples. The samples were then annealed in a thermostated aluminum reaction block for 4 h at 175 °C.

A melt mixed sample was prepared by weighing out PB (0.4 g) and ODA (1.6 g) along with DPD (0.05 wt % of the total weight of the batch) and AA (0.01 wt % of the total weight of the batch) in a 20 mL vial and heated on a thermostated aluminum reaction block to 60 °C for 24 h. The vial was shaken periodically to ensure the homogeneity of the mixture after which it was placed in a vacuum oven at 40 °C for 2 h to remove any trapped air. The degassed sample (maintained at the elevated temperature) was then poured into a circular spacer (1 mm thick, 60 mm inner diameter, and 75 mm outer diameter) preheated to 50 °C on thermostated caged platens (Low Temp Plate LT2) and pressed using a compression molder (Dake) at 175 °C, under an applied load of 40 kg/cm^2 for 4 h. This sample was referred to as PB-0.66ODA-M, where M denotes melt mixed sample.

High-temperature annealing of neat ODA was carried out by measuring 1 g of ODA, DPD (0.05 wt % of the total weight of the sample), and AA (0.01 wt % of the total weight of the sample) in a 20 mL silicone septa-capped vial. This sample was referred to as ODA-R,I. Another control experiment was carried out by measuring 1 g of ODA in a 20 mL silicone septa-capped vial. This sample was referred to as ODA-R. Both of these samples were placed in a thermostated aluminum reaction block, were heated to 60 °C until ODA melted, and then were sparged with nitrogen gas for 15 min to degas the samples. The samples were then annealed in a thermostated aluminum reaction block for 4 h at 175 °C.

2.3. Characterization. Characterization was carried out on the annealed samples after curing. The sol fraction was only removed to determine the gel content of the samples and the equilibrium swelling ratio and to characterize the mechanical properties of the gel samples.

2.3.1. Nuclear Magnetic Resonance Spectroscopy. ^{1}H nuclear magnetic resonance experiments (proton NMR) were performed on a Varian NMR Spectrometer-500 instrument at 500 MHz (32 scans) using $CDCl_3$ as the solvent or on a Varian NMR Spectrometer-300 instrument at 300 MHz (32 scans) using $CDCl_3$ as the solvent.

2.3.2. Gel Permeation Chromatography. The molecular weight of the polymers was determined using a Tosoh SEC HLC-8320 Quad Detector gel permeation chromatography (GPC) instrument equipped with a refractive index detector (RI). The samples were prepared in THF at a concentration of (2.0−4.0) mg/mL, and the molecular weights were calculated based on polystyrene standards.

2.3.3. Fourier Transformed Infrared Spectroscopy. The attenuated total reflection Fourier transform infrared (ATR-FTIR) spectral analysis was performed using the Nicolet 6700 FTIR spectrometer to analyze the extracted sol of the cross-linked polymer. The FTIR spectrum was analyzed within a range of 400 to 4000 cm^{-1}, with 32 scans at a resolution of 4 cm^{-1}.

2.3.4. Determination of the Gel Content. A rectangular sample (4 cm × 4 cm × 0.8 cm) was cut from a cured disk and weighed to record the sample's initial weight (W_0). The sample was then immersed in 10 mL of toluene for 48 h to extract the sol fraction replacing the toluene after 24 h, after which the sample was dried at 80 °C under vacuum in a vacuum oven overnight to determine the sample's final weight (W_f). Solvent extraction was performed at room temperature and 70 °C. The gel content for ODA-R and ODA-R was carried out by soaking the annealed products in 10 mL of THF (at RT) to extract any sol fraction present.

The gel fraction (G), therefore, was determined as

$$G = \frac{W_f}{W_0} \tag{1}$$

The sol fraction was dried by first removing the solvent using a rotary evaporator (Buchi-R200) at 40 °C (77 mbar of Hg) and then dried by placing the sample at 80 °C under vacuum in a vacuum oven overnight.

2.3.5. Determination of the Equilibrium Swelling Ratio. The sol-extracted sample was weighed to record the initial weight (W_i). The sample was then immersed in toluene at room temperature to determine the weight of the swollen sample (W_s). The swollen weight was recorded at periodic intervals of time until the swollen weight plateaued (60−65 h). The swelling ratio of the gels (SR) was determined as

$$\mathrm{SR} = \left(\frac{W_s - W_i}{W_i}\right) \tag{2}$$

2.3.6. Differential Scanning Calorimetry (DSC). PB-*x*ODA, ODA, ODA-R, ODA-R,I, and PB-*x*EI samples were loaded and sealed in hermetic aluminum pans and characterized either by a Discovery DSC 250 (TA instrument) or DSC 200 (TA instrument). The samples were initially equilibrated at −70 °C (PB-*x*ODA) or 0 °C (ODA, ODA-R, ODA-R,I, and PB-*x*EI) followed by two heating−cooling cycles between −70 and 70 °C (PB-*x*ODA) or 0 and 60 °C (ODA, ODA-R, ODA-R,I, and PB-*x*EI), at a rate of 10 °C/min. The purging rate of the nitrogen gas was 40 mL min^{-1}. All thermal properties were determined from the second heating run.

2.3.7. Mechanical Properties. The samples' mechanical properties were analyzed using a Q800 DMA (TA Instruments) at room temperature (RT) and at 70 °C. All the samples tested at elevated temperatures were equilibrated at 70 °C for 2 min before starting the experiment. A constant preload force of 0.001 N was applied throughout the experiment. The rectangular film specimens were programmed in a DMA strain rate mode to undergo uniaxial stretching at a rate of 0.1 mm/min to a final clamp separation length of 25 mm for the uniaxial tensile tests.

The storage modulus was analyzed by isochronal temperature sweeps using a Q800 DMA (TA Instruments) performed at a heating rate of 10 °C/min at a frequency of 1 Hz (applied strain = 0.1%) over a temperature range of room temperature to 70 °C.

Stress relaxation experiments were carried out at 70 °C using a Q800 DMA (TA Instruments, USA) at an applied constant strain of 50% and then monitoring the stress for 60 min. The stress relaxation curves were expressed as $(\sigma(t)/\sigma_0)$, where $\sigma(t)$ is the stress during relaxation and σ_0 is the initially applied stress.

2.3.8. X-ray Scattering. SAXS and WAXS measurements on annealed PB-*x*ODA samples at room temperature and at 70 °C and on a stretched sample (PB-0.66ODA, heated to 70 °C, strained to 90%, fixed at room temperature) at room temperature were performed with a Xenocs Xeuss 3.0 instrument using a Cu Kα source (λ = 1.54 Å) with a beam cross section of 0.5 mm × 0.5 mm at the specimen position for the SAXS experiments and a beam cross section of 0.7 mm × 0.7 mm at the specimen position for the WAXS experiments. The acquisition time for each specimen was 300 s for SAXS and 180 s for WAXS.

2.3.9. Shape Memory Properties. Stress-controlled shape memory properties were measured using a DMA (TA Instruments Q800). The sample's shape memory cycle was carried out as follows: The sample was heated to 70 °C at 10 °C min^{-1} and held at that temperature for 2 min. Then, the stress was ramped to 0.07−0.35 MPa at 0.05 MPa min^{-1} once the sample temperature reached 70 °C. Shape fixing was then conducted by ramping the temperature to 20 °C at 10 °C min^{-1} and holding at that temperature for 5 min. Once reaching 20 °C, the stress was dropped to 0.00 MPa. The shape recovery was conducted by ramping the temperature to 70 °C at 10 °C min^{-1} and holding it for 2 min. The % fixity and the % recovery were defined as

$$\%\text{fixity} = \frac{\varepsilon_f}{\varepsilon_a} \times 100\% \tag{3}$$

https://doi.org/10.1021/acsapm.3c00319
ACS Appl. Polym. Mater. XXXX, XXX, XXX−XXX

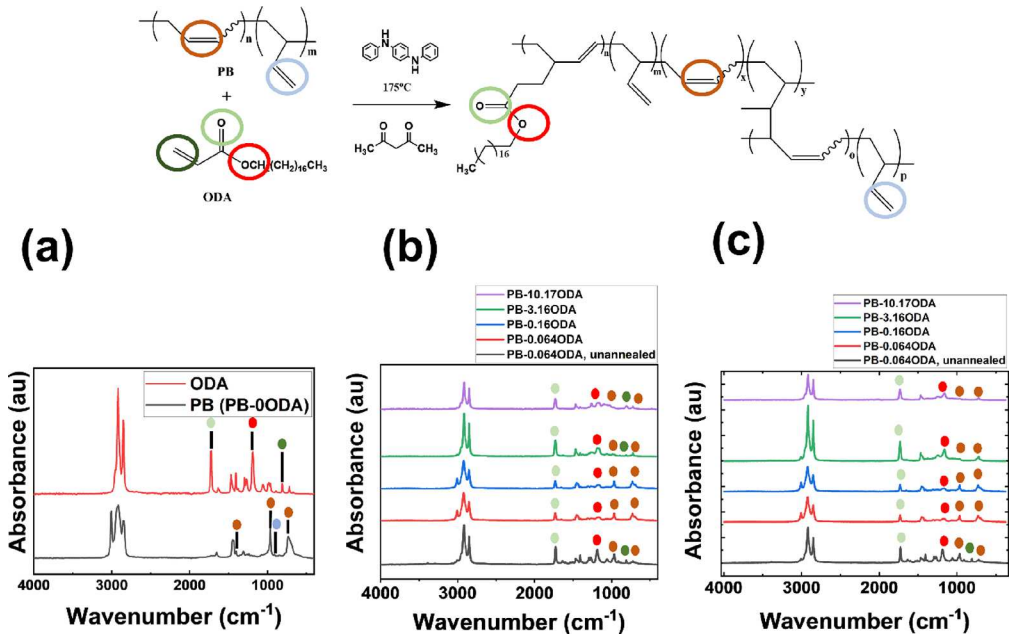

Figure 1. (a) FTIR spectra of unannealed PB (PB-0ODA) and unannealed ODA. (b) FTIR spectra of unannealed PB-0.064ODA and gel fractions of PB-*x*ODA (sol extracted at RT). (c) FTIR spectra of unannealed PB-0.064ODA along with gel fractions of PB-*x*ODA (sol extracted at 70 °C).

$$\%\text{recovery} = \frac{\varepsilon_a - \varepsilon_r}{\varepsilon_a} \times 100\% \quad (4)$$

where ε_a is the applied strain, ε_f is the fixed strain, and ε_r is the residual strain obtained from the DMA stress−strain−temperature curves.

To investigate the shape memory properties of samples over multiple cycles and to observe the effect of blooming on the shape memory properties during each cycle, the shape memory properties of annealed PB-0.66ODA were measured manually using a rectangular-shaped sample (7 cm × 2 cm × 0.8 cm) cut from the cured film. Two lines approximately 3 mm apart were marked using a permanent marker. The shape memory cycle for this experiment comprises (i) heating the material to 70 °C using a hot water bath for 2 min; (ii) stretching the material to approximately 50% strain manually using two tweezers and holding it for 2 min; (iii) cooling the material by quenching in the air at room temperature for 10 min; (iv) removing the load and measuring the shape fixity; and (v) heating the material to 70 °C using a hot water bath for 5 min to measure the shape recovery.

The length between the marked lines was measured after every step of the shape memory cycle to give the length of the initial sample (L_i), the length after cooling at room temperature (while keeping the load on) (L_a), the length after removing the load for 2 min under ambient conditions (L_f), and the length after recovery (L_r). The initial strain (ε_i), applied strain (ε_a), fixed strain (ε_f), and residual strain (ε_r), in this case, were calculated as

$$\varepsilon_x = \frac{L_x - L_i}{L_i} \quad (5)$$

where L_x is L_i, L_a, L_f, or L_r, with the same subscript as ε_x.

With these strains, the % fixity and the % recovery were calculated from eqs 3 and 4 as described above.

The recovered sample was then placed on a paper towel to blot excess water and then reweighed, and the process was repeated for a total of 10 shape memory cycles.

The shape memory properties of annealed PB-*x*EI films were measured manually using a rectangular-shaped sample (6 cm × 1.5 cm ×2 cm) cut from the cured film. The shape memory cycle was carried out the same as for annealed PB-0.66ODA described above. The shape memory properties of samples over multiple cycles and to observe the effect of blooming on the shape memory properties during each cycle were also carried out on annealed PB-0.76EI with a similar procedure as carried out for PB-0.66ODA described above.

3. RESULTS AND DISCUSSION

3.1. Thermal Annealing of PB-*x*ODA. Heating PB and ODA at 175 °C resulted in the formation of cross-linked material. We believe that two main reactions occurred during annealing, the grafting of the ODA to the PB backbone and the cross-linking of the PB. As previously reported by Ritter and co-workers, ODA is grafted to polybutadiene oligomers via an Alder-ene reaction.[23] The evidence for this grafting reaction is discussed first. After annealing, the cross-linked gel fraction was separated from the sol fraction by extraction of the sol fraction in toluene, a good solvent. Figure 1a shows the spectra of the individual PB (PB-0ODA) and ODA components, and Figure 1b shows the spectra of the initial (i.e., unannealed) PB-0.064ODA blend and of gel fractions (extracted at RT) of the annealed, cross-linked blends at different ODA loadings. The C−H peaks at 740, 911, 970, and 1408 cm^{-1} confirm the presence of the polybutadiene main chain in the gels.[26] The grafting of the octadecyl acrylate is inferred via the two characteristic peaks of the ester group appearing at 1730 and 1180 cm^{-1} from the C═O and C−O groups, respectively, and the absence of the ODA vinyl double peak at 812 cm^{-1} at lower ODA loading.[27] At higher ODA loading (PB-3.16ODA and PB-10.17ODA), there is a peak at 812 cm^{-1}, indicating the presence of free ODA in the gel fraction that could not be removed during the sol extraction process. The sol extraction process was repeated at 70 °C, and the FTIR results indicate that all unreacted ODA was removed over the same range of ODA loadings (Figure 1c).

Butyl acrylate is known to free-radically polymerize in the absence of any added initiator at high temperatures (ca. >180 °C), where it is suggested that initiating free radicals form from reactions between the monomers.[28−30] The analogous reaction in ODA would produce poly(octadecyl acrylate), which could also graft to the PB and potentially form cross-links. Two control experiments were performed where ODA was

https://doi.org/10.1021/acsapm.3c00319
ACS Appl. Polym. Mater. XXXX, XXX, XXX−XXX

thermally annealed under nitrogen at 175 °C for 4 h in the presence (ODA-R,I) and absence (ODA-R) of the free radical inhibitor package of DPD and AA. Both products were completely soluble in THF ($G = 0$), indicating the absence of any gel network formation. The dried products were characterized by GPC, NMR, and DSC (Figure 2). The

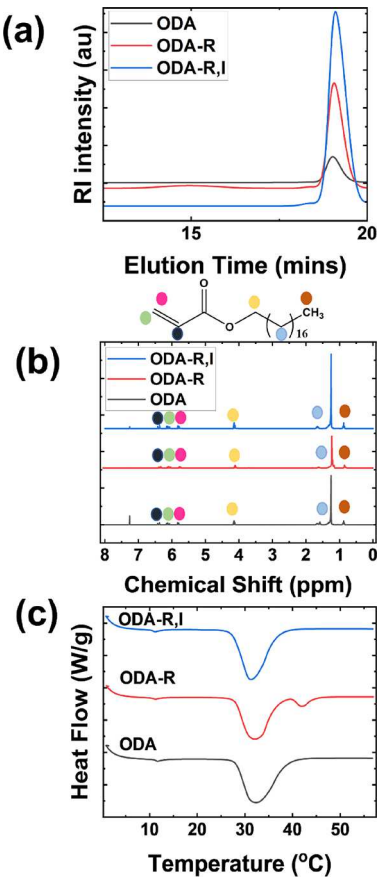

Figure 2. (a) GPC traces, (b) proton NMR shifts, and (c) DSC heating curves of the sol fraction (extracted at RT) of high-temperature (175 °C) annealed ODA samples (ODA-R and ODA-R,I) and unreacted ODA (ODA).

GPC traces (Figure 2a) show a large peak at long elution time identified as ODA. In annealed ODA-R and annealed ODA-R,I, there is a small shoulder at shorter elution time on the ODA peak, which could be due to dimerization in the process of autoinitiation. The annealed ODA-R,I showed a flat baseline at a shorter elution time, indicating that no measurable PODA was formed, which indicates that the radical inhibitors were effective at preventing polymerization at the concentration used. In the absence of an inhibitor, annealed ODA-R shows a broad peak at short elution time, indicating the formation of some PODA. The NMR traces (Figure 2b) for ODA, annealed ODA-R, and annealed ODA-R,I are nearly identical suggesting little formation of PODA. Setting the integral area of the peak for the methyl group in ODA (δ = 0.81, $-CH_3$) to 3, the integral areas for (δ = 4.09, OCH_2; δ = 5.75, $=CH-$; δ = 6.01, $=CH_2$; δ = 6.36, $=CH_2$) were determined. Table S1 (Supporting information) lists the integral areas of these peaks. The integral areas for ODA and annealed ODA-R,I are almost identical, while there is a small reduction (2−5%) in the integral area of the vinyl peaks in annealed ODA-R consistent with the formation of a small amount of polymer. The DSC heating curves (Figure 2c) show a single melting peak for ODA[31] and annealed ODA-R,I, while annealed ODA-R shows an additional melting peak at 42 °C (peak), attributed to the PODA.[32] As this inhibitor package was used in the preparation of all the samples at the same concentration based on the weight of the sample, it is assumed that the polymerization of ODA to form PODA is negligible and the incorporation of ODA in the gel fraction is due to grafting of the ODA monomer.

The FTIR spectra for sol fractions (extracted at RT) for different annealed PB-xODA samples ($x \leq 20.6$) are shown in Figure S1 (Supporting information). They exhibit the characteristic ODA peak at 1730 cm^{-1}, while the characteristic PB peak at 3007 cm^{-1} is absent except for the PB-20.6ODA sample, which has a negligible gel fraction, indicating that the sol fraction is composed of ODA, except when the gel fraction is negligible. The proton NMR of different sol fractions (extracted at RT) ($x \leq 20.6$) Figure S2 (Supporting Information) along with the GPC of different sol fractions (extracted at RT) ($x \leq 3.16$) Figure S3 (Supporting Information) also supports that the sol fraction was comprised solely ODA when a non-negligible gel fraction was present. While PB has the characteristic proton shifts at 5.38 ppm ($=$CH-) and 2.07 ppm ($-CH_2-$), these peaks were absent in the sol fractions examined by NMR, except for the PB-20.6ODA sample. In the GPC traces, only a peak at the elution time of the ODA was observed in the sol samples, except for the PB-20.6ODA sample (Figure S3). The elution time of the PB in the PB-20.6ODA shifts to a shorter time, indicating a larger hydrodynamic volume, consistent with the grafting of ODA onto the PB backbone.

We believe that the cross-linking of the samples occurred due to cross-linking reactions between PB chains. Cross-linking reactions between 1,2 and 1,4 PB units were first observed by Grassie and Heaney on low vinyl (9−14%) PB annealed under vacuum at 230 °C.[33] The addition of the terminal carbon of the 1,2 unit to the allylic carbon of the 1,4 unit resulting in the loss of the 1,2 unsaturation was proposed based on the previous work of Golub and Sung.[34] This was assumed by Grassie and Heaney to be a first-order reaction in the concentration of 1,2 units. This reaction was subsequently revisited by Golub, and an alternative reaction was proposed where the 1,2 unit adds to the allylic carbon on the 1,4 unit through the internal carbon ($-CH{=}CH_2$) on the 1,2 unit producing a pendant methyl group.[35] In addition, Golub observed this reaction to be second-order in the 1,2 unit concentration, although an explanation was not provided for this observation in low vinyl PB. Subsequent ^{13}C NMR studies by Doskočilová et al.[36] and later Ziaee and coworkers[37−39] identified that the 1,2 unit adds at a 1,4 unit adjacent to a 1,2 unit producing the same structure as proposed in Golub's later work.[34] This reaction scheme would explain the observation of a second-order reaction in 1,2 concentration even though only one 1,2 unit adds to the PB chain. Annealing neat PB at 175 °C for different times, FITR measurements showed the ratio of the peak areas from the 1,2-characteristic peak at 911 cm^{-1} to the 1,4-characteristic peak at 1408 cm^{-1} decreased with time, indicating the disappearance of the 1,2 units. The 1,2 unit peak area normalized by the 1,4 unit peak area are plotted vs time as first- and second-order plots in Figure S4 (Supporting Information), where the change in the 1,4 is assumed to be negligible and therefore used to remove any sample-to-sample variation in the 1,2 unit concentration other than its

https://doi.org/10.1021/acsapm.3c00319
ACS Appl. Polym. Mater. XXXX, XXX, XXX−XXX

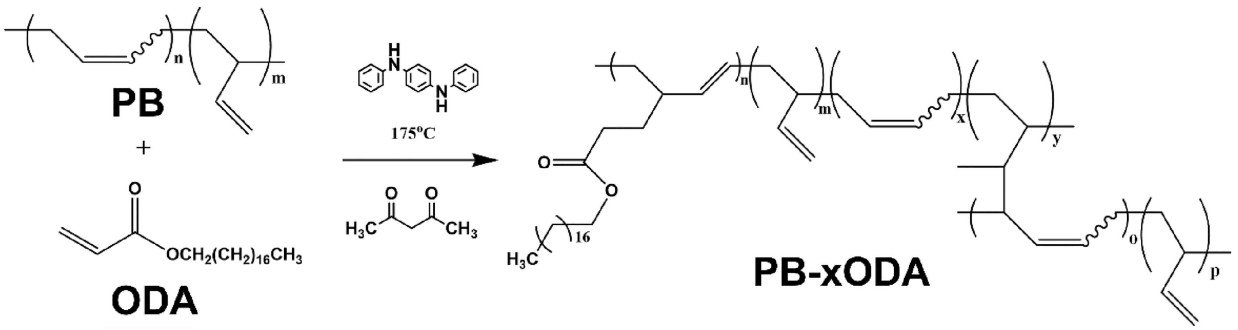

Figure 3. Proposed route to cross-linked PB-*x*ODA polymers through thermal annealing (at 175 °C) of mixtures of high *cis*-1,4-PB and ODA.

consumption in the cross-linking reaction. The second-order plot gives a much better linear fit in agreement with the previous observation of a second-order reaction in 1,2 unit concentration.

Based on the evidence for only ODA grafting and PB cross-linking and prior investigation of these two reactions, the proposed structure of the grafted and cross-linked polymer is shown in Figure 3, where the ODA grafting and cross-linking between 1,2 and 1,4 repeat units are the dominant reactions. In the blend, the reaction of the ODA with the 1,2 PB units would compete with this cross-linking. However, based on Hoffman's work, hydrogen abstraction from the least substituted allylic position is kinetically favored.[40] This, coupled with the much higher concentration of 1,4 units to 1,2 units, would favor the ene reaction between the ODA and 1,4 units. Similarly, cyclization reactions between 1,2 units are also unlikely due to the low 1,2 unit concentration, favoring the addition reaction between 1,2 and 1,4 units.

3.2. Analysis of the Gel Fraction and the Swelling Ratio of Annealed PB-*x*ODA. Figure 4a shows the gel fraction (G) of the annealed PB-*x*ODA vs the molar ratio of ODA to PB repeat units, [ODA]/[B] obtained from room temperature and 70 °C sol extraction. The gel fractions are slightly lower at 70 °C compared to room temperature. The gel fraction of PB-0ODA was recorded to be 0.995 (at RT) and 0.994 (at 70 °C). The gel fraction shows a steady decrease with an increase in [ODA]/[B]. As no PB was detected in the sol fraction at [ODA]/[B] < 20.6, the reduction in the gel fraction is attributed to the presence of unreacted ODA.

Based on the FTIR results in Figure 1, it is assumed that all unreacted ODA is extracted into the sol at 70 °C and the remaining gel is only ODA grafted PB. The fraction of ODA reacted (i.e., grafted), $f_{\text{ODA-R}}$, was calculated as

$$f_{\text{ODA-R}} = 1 - \frac{w_s}{w_{\text{ODA}_o}} = 1 - \left(\frac{w_s}{w_o}\right)\left(\frac{w_o}{w_{\text{ODA}_o}}\right) = 1 - (1 - G)\left(1 + \frac{[\text{B}]}{[\text{ODA}]}\frac{M_B}{M_{\text{ODA}}}\right) \quad (6)$$

where w_s is the weight of the sol fraction extracted at 70 °C, w_{ODA_o} is the initial weight of ODA in the sample, G is the gel fraction for the extraction run at 70 °C, and M_B and M_{ODA} are the molar masses of the PB repeat unit (M_B = 54 g/mol) and the ODA (324.5 g/mol), respectively. The fraction of PB repeat units grafted with ODA is

$$f_{\text{PB-ODA}} = f_{\text{ODA-R}}\frac{[\text{ODA}]}{[\text{B}]} \quad (7)$$

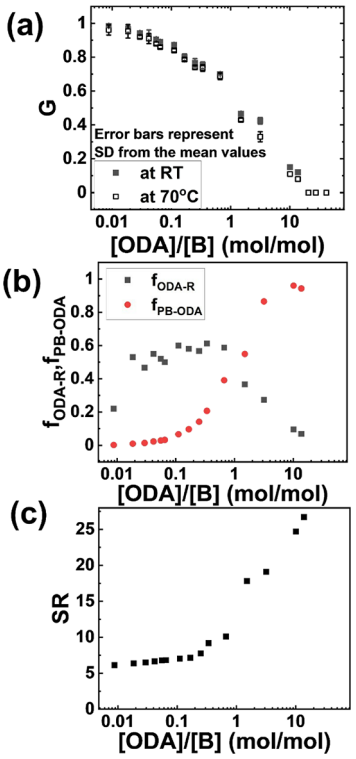

Figure 4. Annealed PB-*x*ODA properties vs [ODA]/[B]: (a) gel fraction (G) at room temperature (RT) and at 70 °C sol extraction; (b) fraction of ODA ($f_{\text{ODA-R}}$) reacted and the fraction of PB repeat units grafted with ODA ($f_{\text{PB-ODA}}$), calculated from eqs 6 and 7 where G was taken at 70 °C; and (c) swelling ratio (SR) at RT.

These two quantities are plotted vs [ODA]/[B] in Figure 4b. The fraction of PB repeat units grafted increases monotonically with [ODA]/[B]. The efficiency of the grafting is around 50−60% of the ODA reacting at ratios of [ODA]/[B] < 1 and decreases with a further increase in the stoichiometric excess of [ODA].

The swelling ratio (SR) vs [ODA]/[B] plotted in Figure 4c shows the opposite trend of the gel fraction, indicating a reduction in the cross-link density with increasing ODA concentration. ODA would also act as a solvent in the PB cross-linking reaction, which in addition to diluting the concentration of PB chains would influence the PB chain dimensions (expanding with decreasing PB concentration), the effective entanglement molecular weight (increasing with decreasing PB concentration), and the amount of PB chain overlap (decreasing with decreasing PB concentration).[41] Each factor would contribute to a higher swelling ratio due to

https://doi.org/10.1021/acsapm.3c00319
ACS Appl. Polym. Mater. XXXX, XXX, XXX−XXX

expanded chains, less trapped entanglements, and more intrachain cross-linking with decreasing PB concentration. Cross-link density was not determined from the swelling results as the interaction parameter of the ODA-grafted PB with toluene is not known. Table S2 (Supporting Information) lists the quantitative values of G (RT and 70 °C), $f_{ODA\text{-}R}$, $f_{PB\text{-}ODA}$, and SR.

At [ODA]/[B] ≥ 20.6, no gel fraction is observed. Figure S2 (Supporting Information) shows the NMR spectra of the sol fraction of PB-20.6ODA (G = 0), and the presence of both PB and ODA was observed. This is likely due to a crossover from predominately interchain cross-linking to intrachain cross-linking as the solution approaches the critical overlap concentration. The critical overlap concentration, c^*, is related to the intrinsic viscosity $[\eta]$ of the solution as[42]

$$c^* = \frac{0.77}{[\eta]} \tag{8}$$

where the intrinsic viscosity is given by the Mark−Houwink equation as

$$[\eta] = KM^a \tag{9}$$

For *cis*-1,4-PB (M_w/M_n in the range of 3.0 ± 0.5 and M_n about (150−200) × 10^3 g/mol) in THF at 40 °C, the Mark−Houwink parameters were found to be a_{PB} = 0.580−0.6, average = 0.59 and K_{PB} = 8.0−9.0 × 10^{-2} mL/g, average = 8.5 × 10^{-2} mL/g.[43] M_{PB} is estimated from the PS standard-based molecular weight of the PB[44]

$$M_{PB} = \left(\frac{K_{PS}}{K_{PB}}\right)^{1/1+a_{PB}} \times (M_{PS})^{1+a_{PS}/1+a_{PB}} \tag{10}$$

where the weight average molecular weight of the polymer (455,000 g/mol) is used for M_{PS} as this is closer to the viscosity average molecular weight.[45] Using a_{PS} = 0.73 and K_{PS} = 1.05 × 10^{-2} (mL/g) (with THF as an eluent at 40 °C),[46] eq 10 gives M_{PB} = 384,580 g/mol.

For the calculation of intrinsic viscosity using eq 9, the Mark−Houwink parameters of PB in toluene (at 25 °C) of a_{PB} = 0.750 and K_{PB} = 2.36 × 10^{-2} mL/g[40] and in THF were used to estimate c^* over a range of good solvent conditions. Plugging these values in eq 9 gives $[\eta]$ = 364.5 g/mL and c^* = 2.1 × 10^{-3} g/mL in toluene and $[\eta]$ = 167.7 g/mL and c^* = 4.6 × 10^{-3} g/mL in THF.

The critical overlap concentration was converted to an ODA:PB repeat molar ratio by the following equation (Supporting Information, appendix 1)

$$\frac{[ODA]^*}{[B]^*} = \frac{\left(1 - \frac{c^*}{\rho_B}\right)}{\frac{c^*}{\rho_{ODA}}\frac{M_{ODA}}{M_B}} = \frac{\left(1 - \frac{c^*}{0.91}\right)}{\frac{c^*}{0.86}\frac{M_{ODA}}{M_B}} \tag{11}$$

where [ODA] and [B] are the molar concentrations, M_{ODA} (324.5 g/mol) and M_B (54 g/mol) are the molar masses of the ODA and PB repeat unit, respectively, and ρ_{PB} and ρ_{ODA} are the density of *cis*-PB and ODA, respectively. Assuming ρ_{PB} = 0.91 g/cm^3[47] and ρ_{ODA} = 0.86 g/cm^3,[48] the range of [ODA]*/[PB]* was calculated to be 31.1 (THF) to 67.9 (toluene). As the difference in solubility parameters between PB and ODA is more similar to that of PB and toluene, the overlap concentration is likely closer to the value calculated based on toluene. As a number of approximations were made in this calculation, it is not assumed to be quantitative but gives a reasonable order of magnitude estimate of the critical overlap concentration.

3.3. Thermal Properties of the Annealed PB-*x*ODA.

The results of the DSC analysis of the annealed PB-*x*ODA blends are shown in Figures 5 and 6. The transition

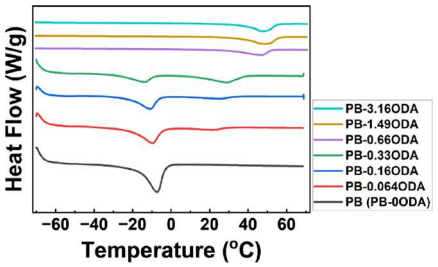

Figure 5. DSC second heating curves of PB-*x*ODA (heating/cooling rate = 10 °C/min).

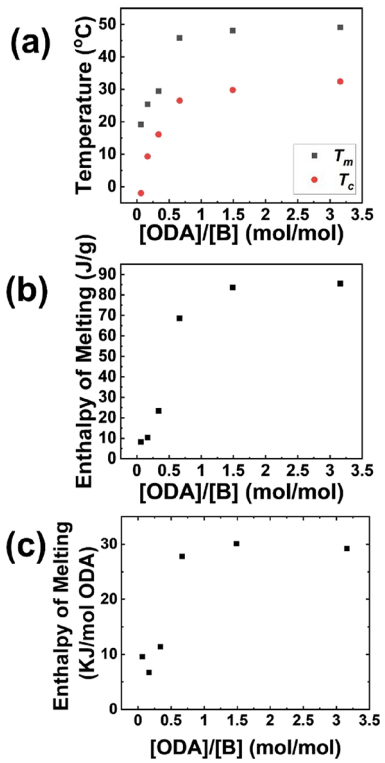

Figure 6. Variation of the PB-*x*ODA thermal properties vs [ODA]/[B]: (a) peak melting temperature (T_m) and the peak crystallization temperature (T_c), (b) enthalpy of melting (J/g) (DSC heating/cooling rate = 10 °C/min), and (c) enthalpy of melting of PB-*x*ODA expressed as kJ/mol ODA.

temperatures are presented in the Supporting Information (Tables S3 and S4, Supporting Information). At low [ODA]/[B], two melting peaks are observed corresponding to the crystallization of the PB backbone (<0 °C) and the crystallization of the mixture of grafted and free ODA. As [ODA]/[B] decreases, the ODA melting temperature decreases. The melting point depression is consistent with other comb-like polyacrylate and polymethacrylate copolymers having crystallizable *n*-octadecyl side chains, while the presence of a single melting peak is consistent with blends of poly(*n*-octadecyl acrylate) with *n*-octadecanoic acid and *n*-aliphatic hydrocarbons[49−54] due to the combined effects from the

https://doi.org/10.1021/acsapm.3c00319
ACS Appl. Polym. Mater. XXXX, XXX, XXX−XXX

entropic gain of mixing the chemically different units, decreasing ODA concentration, and the co-crystallization of ODA with the PB-*x*ODA that regulates the crystal growth and thereby the melting temperature and the enthalpy of melting. The enthalpy of melting (ΔH_m) in kJ/mol of ODA was calculated as

$$\Delta H_m \text{ (kJ/mol ODA)} = \frac{\Delta H_m(\text{J/g}) M_{ODA}}{w_{ODA}(1000 \text{ J/kJ})} \quad (12)$$

where w_{ODA} is

$$w_{ODA} = \frac{[\text{ODA}]M_{ODA}}{[\text{ODA}]M_{ODA} + [\text{B}]M_B} \quad (13)$$

and is plotted in Figure 6c. At high ODA fraction, ΔH_m (kJ/mol ODA) is relatively constant and similar to the enthalpy of melting of PODA (29.0 kJ/mol).[27] However, the rapid drop in the enthalpy of melting at lower ODA concentration indicates that more ODA is present in the amorphous regions of the material.

As shown in Figure S5 (Supporting Information), the gel fractions of annealed PB-*x*ODA show a similar melting temperature. Therefore, the grafted ODA (on the PB chains) and the free ODA form a single melting/crystallization temperature that increases with the increase in the [ODA]/[B] molar ratio. The grafted ODA and the free ODA are expected to have similar melting temperature profiles owing to the similar length of the crystallizable ODA segments.[55,56]

3.4. Mechanical Properties of the Annealed PB-*x*ODA.

Samples of five annealed PB-*x*ODA at different [ODA]/[B] mole ratios (PB (PB-0ODA), PB-0.064ODA, PB-0.16ODA, PB-0.33ODA, and PB-0.66ODA) were chosen to study the physical and mechanical properties of annealed PB-*x*ODA. The tensile properties of annealed PB-*x*ODA samples are shown in Figure 7a (room temperature) and Figure 7b (70 °C) for both the annealed and sol-extracted (at room temperature) samples. Table S5 (Supporting Information) lists the quantitative mechanical properties (storage modulus at 25 °C, storage modulus at 70 °C, maximum strain at RT, maximum strain at 70 °C, and the Mooney−Rivlin parameters) of the annealed and sol-extracted annealed PB-*x*ODA polymers. Samples with higher [ODA]/[B] show poor room-temperature properties (such as being brittle and easily crumbled when deformed with a small load), making them poor candidate materials for shape memory polymers.

At room temperature, the samples become stiffer and fail at lower strain with increasing [ODA]/[B] ratio, while at 70 °C (above the T_m of ODA domains), the samples become softer and show failure at lower strain with increasing [ODA]/[B] ratio. The ODA, both grafted and free, acts as a reinforcing filler and is likely a site for crack initiation at low temperature giving rise to higher modulus and lower strain to failure. At elevated temperature, the ODA acts as a diluent, lowering the modulus and decreasing the strain to failure. The sol-extracted samples show a reduction in the effects of the ODA, namely, a lower modulus and higher strain to failure at room temperature and a higher modulus and higher strain to failure at elevated temperature. As almost no sol was extracted in the annealed PB (PB-0ODA) samples, the variation in these samples from the annealed to sol-extracted is likely due to sample-to-sample variation.

Figure 7c shows the isochronal temperature sweeps of the annealed PB-*x*ODA. At higher ODA loading (PB-0.33ODA and PB-0.66ODA), a sharp drop in the storage modulus is consistent with the melting of the ODA crystals above room temperature.

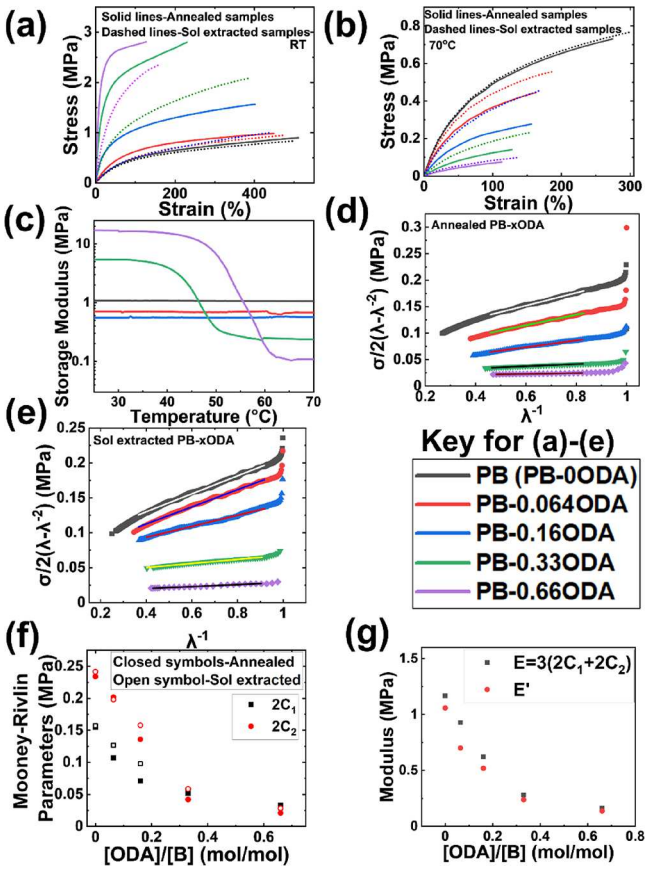

Figure 7. (a) Room temperature (RT) stress−strain curves of annealed PB-*x*ODA and sol extracted (RT extraction) PB-*x*ODA (stretching rate of 0.1 mm/min); (b) 70 °C stress−strain curves of annealed PB-*x*ODA and sol extracted (RT extraction) PB-*x*ODA (stretching rate of 0.1 mm/min); (c) storage modulus vs temperature for PB-*x*ODA (heating rate of 10 °C/min, frequency of 1 Hz, and applied strain = 0.1%). (d) Mooney−Rivlin plots obtained from the stress strain curves at 70 °C (Figure 7b) for annealed PB-*x*ODA. (e) Mooney−Rivlin plots obtained from the stress strain curves at 70 °C (Figure 7b) for sol-extracted PB-*x*ODA. (f) Mooney−Rivlin parameters ($2C_1$ and $2C_2$) vs [ODA]/[B] for both annealed PB-*x*ODA and sol-extracted PB-*x*ODA. (g) Comparison of the 70 °C plateau storage modulus (E') from the temperature sweeps and the elastic modulus (E) obtained from the Mooney−Rivlin equation ($E = 3(2C_1 + 2C_2)$), for annealed PB-*x*ODA at 70 °C.

The stress−strain curves at 70 °C (Figure 7b) were replotted to calculate the Mooney−Rivlin parameters. The linear region in Figure 7d,e was used to fit the Mooney−Rivlin equation,[57−59]

$$\frac{\sigma}{\left(\lambda - \frac{1}{\lambda^2}\right)} = 2C_1 + \frac{2C_2}{\lambda} \quad (14)$$

where σ is the stress, λ is the extension ratio ($\lambda = 1 + \varepsilon$), and $2C_1$ and $2C_2$ are the fitting parameters. The fits are shown in Figure 7d,e, and the parameters $2C_1$ and $2C_2$ are plotted in Figure 7f for both the annealed and sol-extracted samples.

$2C_1$ should scale with the modulus predicted by the ideal rubber model, while $2C_2$ has been attributed to entanglement effects and topological constraints in tensile measure-

https://doi.org/10.1021/acsapm.3c00319
ACS Appl. Polym. Mater. XXXX, XXX, XXX−XXX

ments.[60−67] Figure 7g also shows the plateau modulus (E') obtained from the temperature sweep results (Figure 7c) along with the elastic modulus (E) obtained from the Mooney−Rivlin equation at the limit of $\lambda \rightarrow 1$ where $E = 3(2C_1 + 2C_2)$.[60] The agreement between $2C_1$ and the plateau modulus improves with increased ODA loading. At low ODA loading, the PB is likely highly entangled, whose contribution to the modulus may vary between the two experiments due to viscoelastic effects. Both $2C_1$ and $2C_2$ decrease with increased ODA loading. This is attributed to a lower cross-link density (for $2C_1$) and a lower entanglement density (for $2C_2$) due to the dilution by the grafted and free ODA.

At 70 °C, $2C_1$ may be used to calculate the strand density of the cross-linked networks in the annealed PB-xODA ($(\upsilon_e/V_oN_{av})_{an}$) and sol-extracted PB-$x$ODA ($(\upsilon_e/V_oN_{av})_{sol\ ext}$) samples, based on the phantom network model as[67]

$$\frac{\upsilon_e}{V_oN_{av}} = \frac{2C_1}{RT}\left(1 - \frac{2}{f}\right) \tag{15}$$

where υ_e is the number of elastically effective strands in the sample, V_0 is the initial volume of the polymer, N_{av} is Avogadro's number, R is the universal gas constant (8.314 J·mol^{-1}·K^{-1}), T is the temperature, and f is functionality of the network junctions assumed to be $f = 4$ for these samples.

For the annealed PB-xODA samples, the strand density is also estimated as

$$\left(\frac{\upsilon_e}{V_oN_{av}}\right)_{an,est} = \frac{2C_{1,PB}}{RT}\left(1 - \frac{2}{f}\right)\phi_{PB} \tag{16}$$

where $2C_{1,\ PB}$ is the Mooney−Rivlin parameter of the PB-0ODA (annealed, pure PB) and ϕ_{PB} is the volume fraction of PB in the annealed, cross-linked sample PB-xODA sample given as

$$\phi_{PB} = \frac{\left(\frac{w_{PB}}{\rho_{PB}}\right)}{\left(\frac{w_{PB}}{\rho_{PB}}\right) + \left(\frac{w_{ODA}}{\rho_{ODA}}\right)} \tag{17}$$

where w_{PB} and w_{ODA} are the weight fractions of PB and ODA used and ρ_{PB} and ρ_{PB} are the densities of ODA (0.86 g/cm^3)[48] and PB (0.91 g/cm^3).[47] This estimate assumes that the degree of polymerization of the PB between cross-links is invariant with [ODA] loading and the ODA chains dilute the strands using a linear rule of mixtures. In the sol-extracted samples, the strand density will increase as the removal of the free ODA collapses the network and is analogous to reduction in strand density by swelling a cross-linked elastomer in a good solvent. The estimated strand density for the sol-extracted sample is

$$\left(\frac{\upsilon_e}{V_oN_{av}}\right)_{sol\ ex,est} = (\phi_{PB\text{-}g\text{-}ODA})^{-1/3}\frac{2C_{1,PB}}{RT}\left(1 - \frac{2}{f}\right)\phi_{PB} \tag{18}$$

where $\phi_{PB\text{-}g\text{-}ODA}$ is the volume fraction of PB grafted with ODA given as

$$\phi_{PB\text{-}g\text{-}ODA} = \frac{(V_{PB}) + (V_{ODA}\text{reacted})}{(V_{PB}) + (V_{ODA})} = \frac{\left(\frac{w_{PB}}{\rho_{PB}}\right) + \frac{(f_{ODA\text{-}R})(w_{ODA})}{\rho_{ODA}}}{\left(\frac{w_{PB}}{\rho_{PB}}\right) + \left(\frac{w_{ODA}}{\rho_{ODA}}\right)} \tag{19}$$

while $(\upsilon_e/V_oN_{av})_{an}$ and $(\upsilon_e/V_oN_{av})_{sol\ ex}$ are plotted as points and $(\upsilon_e/V_oN_{av})_{sol\ ex,\ est}$ and $(\upsilon_e/V_oN_{av})_{an,\ est}$ are plotted as solid lines vs [ODA]/[B] in Figure 8. The quantitative values of

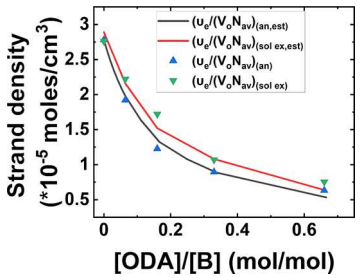

Figure 8. Strand density for annealed PB-xODA and sol-extracted PB-xODA vs [ODA]/[B]. Points calculated from $2C_1$ and eq 15. Solid lines calculated from $2C_1$ for PB (PB-0ODA) and eqs 16 and 18.

these parameters are given in Table S6, Supporting Information. A smooth curve was not obtained for $(\upsilon_e/V_oN_{av})_{sol\ ex,\ est}$ as $f_{ODA\text{-}R}$varies with [ODA]/[B]. The good agreement between the strand densities from eqs 15, 16, and 18 shows that the ODA primarily acts as a diluent and that the average degree of polymerization of PB between cross-links does not vary significantly over the [ODA]/[B] ratio examined in Figure 7. The use of the data from the sol extraction at room temperature introduces some error (increases ϕ_{PB} and $\phi_{PB\text{-}g\text{-}ODA}$ and decreases $2C_1$), but it is likely small as the variation in the gel fraction is a maximum of 3.5% over the ODA concentrations investigated.

3.5. X-ray Characterization of Annealed PB-xODA.

The morphology of the annealed PB-xODA was investigated by wide- and small-angle X-ray scattering (WAXS and SAXS). At room temperature (RT), the WAXS patterns of PB-0.16ODA, PB-0.33ODA, and PB-0.66ODA (Figure 9a) show a peak q = 1.50 Å^{-1} (0.42 nm plane spacing) attributed to the (100) planes in the hexagonally packed ODA crystals formed by the co-crystallization of the grafted and free ODA. This peak is consistent with previous measurements of side-chain crystalline PODA and PODA/octadecanoic acid mixtures where the hexagonally packed, extended alkyl chains are oriented perpendicular to the polymer backbone.[49,53] A broad peak at q = 1.33 Å^{-1} is observed in all of the samples and is attributed to the PB and side-chain spacing in the amorphous regions of the sample as it is observed in the pure PB (PB-0ODA) and the PB-0.66ODA at 70 °C above the melting temperature of the ODA crystals (Figure 9b).[68] Two weak peaks are observed at ca. 0.195 and 0.39 Å^{-1}, corresponding to plane spacings of 3.2 and 1.6 nm. The uncertainty in the peak position is the formation of shoulders in the intensity vs q rather than clear peaks with an intensity maximum. However, clear diffraction rings are observed at this q radius in the 2D images (Supporting Information, Figure 6a). The peak position was estimated from the change in slope of the intensity vs q (Supporting Information, Figure 6b). These

https://doi.org/10.1021/acsapm.3c00319
ACS Appl. Polym. Mater. XXXX, XXX, XXX−XXX

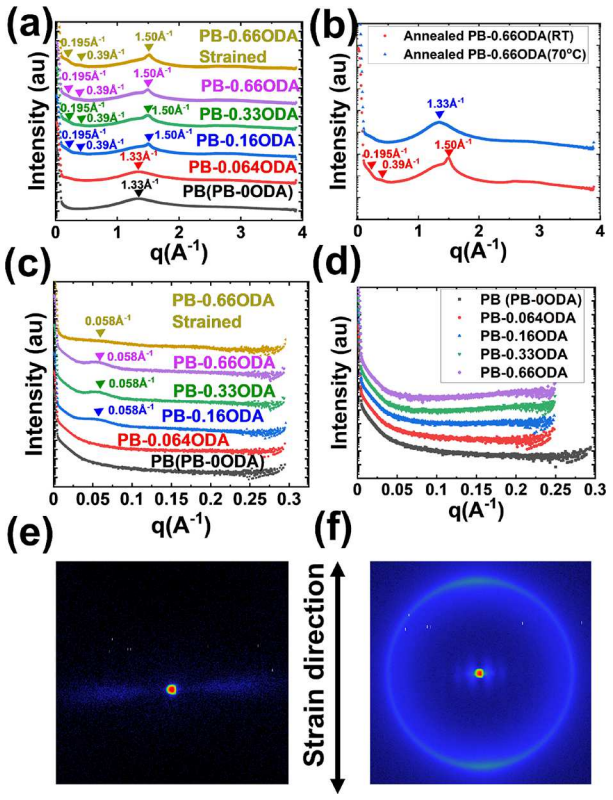

Figure 9. (a–d) Azimuthally averaged intensity vs q: (a) room temperature (RT) WAXS patterns of annealed PB-xODA, (b) RT and 70 °C WAXS patterns of annealed PB-0.66ODA, (c) RT SAXS patterns of annealed PB-xODA, and (d) 70 °C SAXS patterns of annealed PB-xODA. (e) 2D SAXS pattern of stretched annealed PB-0.66ODA and (f) 2D WAXS pattern of stretched annealed PB-0.66ODA.

peaks are attributed to layers of interdigitated alkyl side-chains and the amorphous backbone region (i.e., long-spacing) (as illustrated in Figure 10). Previously, Inomata et al. identified

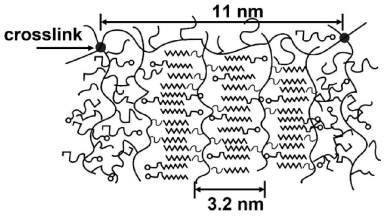

Figure 10. Schematic diagram of the morphology of annealed PB-xODA.

three crystal structures in mixtures of poly[(methyl acrylate)-*stat*-(*n*-octadecyl acrylate)] and *n*-octadecanoic acid, an interdigitating form where side chains from opposing backbones overlap, giving the smallest domain spacing (ca. 3–4 nm); an end-to-end form where side-chains from opposing backbones form a double layer (ca. 5.5 nm), giving the largest domain spacing; and a tilted end-to-end form giving a domain spacing intermediate to the two (ca. 4 nm).[69] The domain spacing was found to increase in the interdigitated form as the fraction of methyl acrylate increased due to an increase in the amorphous volume fraction that must be accommodated between the crystalline side chains. The transition to the end-to-end form allowed more conformational flexibility of the polymer backbone while maintaining a constant interfacial area per long alkyl chain at higher long-alkyl chain loading. More recently, Xiang et al. observed a similar low angle scattering peaks at q_l, $2q_l$, and $3q_l$ for polyacrylates with side-chain lengths of 16 ($d_l = 2\pi/q_l = 2.9$ nm), 18 ($d_l = 3.0$ nm), and 22 ($d_l = 3.4$ nm) carbons.[70] As there are two additional carbons in the side-chain for the grafted ODA, the spacing of 3.2 nm is consistent with the interpolated value for a 20 carbon side-chain. The peak as ca. 0.195 Å^{-1} persists at 70 °C and therefore is attributed to the amorphous interchain spacing above the melting temperature of the ODA crystals.

The SAXS data of annealed PB-xODA (Figure 9c) shows a peak at $q = 0.057$ Å^{-1} for PB-0.16ODA, PB-0.33ODA, and PB-0.66ODA. These are the samples that are crystalline at RT. This peak position corresponds to a domain spacing of 11 nm. Xiang et al. observed a similar peak in the SAXS of polyacrylates with 16 to 22 carbon side-chains with an increasing q_{peak} with increasing chain length (q = 0.074–0.062 Å).[70] This was attributed to the formation of a superstructure with a larger amorphous region alternating with layers of the crystalline side-chains as shown schematically in Figure 10. SAXS on stretched samples by Xiang et al. showed that this domain spacing has the same orientation as the long-spacing of the side-chain crystals (Figure 9e). Its formation was attributed to the high molecular weight of the polymer containing entanglements, which restrict crystallization and were excluded from the crystal. As the PB-0.66ODA shows good shape memory, the sample was stretched (to 90% strain) at elevated temperature (70 °C) and cooled under load (at RT) to fix the deformation. The SAXS and WAXS patterns in Figure 9e,f show a similar orientation, where the backbone chains orient along the stretching direction, the side chains crystallize oriented perpendicular to the backbone, and the superstructure and side-chain crystals form layers oriented in the same direction orthogonal to the stretching direction as shown schematically in Figure 10. In the PB-xODA networks, similar amorphous regions could be located around the cross-linking points. The characterization of the strand density indicated that the degree of polymerization of the PB chain between cross-linking was largely invariant with [ODA]/[B], which could result in a constant domain spacing with the variation in [ODA]/[B] if the amorphous regions are centered around the cross-links and grow at the expense of crystalline regions. The molecular weight between cross-links, M_x, in the annealed PB (PB-0ODA) was calculated as

$$M_x = \frac{\rho_{PB} RT}{2C_1}\left(1 - \frac{2}{f}\right) \tag{20}$$

giving an M_x of 8.4 kg/mol. The distance between cross-links is the average end-to-end distance of the PB chain. Using $\langle R^2\rangle_o/M = 0.758$ Å^2 mol/g gives a root mean square average end-to-end distance ($\langle R^2\rangle_o)^{1/2}$ of 8 nm.[71] A larger domain spacing of 11 nm is obtained if an affine network model is used as

$$M_x = \frac{\rho_{PB} RT}{2C_1} \tag{21}$$

It is also not known the extent to which the crystallization perturbs the end-to-end distance of PB. As this calculation gives a reasonable order of magnitude agreement between the calculated end-to-end distance of strands and the observed domain spacing in SAXS, it provides motivation for further study of the morphology of these materials. Figure 9d shows

https://doi.org/10.1021/acsapm.3c00319
ACS Appl. Polym. Mater. XXXX, XXX, XXX–XXX

the SAXS pattern of PB-*x*ODA at 70 °C and shows no peaks indicating a disordered structure above the melting temperature of the ODA crystals. Interestingly, a SAXS peak at higher q (domain spacings of 3−6 nm) corresponding to the domain spacing between crystal layers, as observed by Inomata et al.[69] and Xiang et al.[70] was not seen. This indicates more variation in the spacing in the direction along the alkyl chains.

3.6. Shape Memory Properties of Annealed PB-*x*ODA. Shape memory testing was conducted using a dynamic mechanical analyzer applying uniaxial elongation. Figure S7 (Supporting Information) shows the stress-controlled SMP cycles of the annealed PB-*x*ODA and Figure 11a shows the results. A complete recovery was observed over the range of varying [ODA]/[B] mole ratios, indicating that the elastic energy stored in the network during the stretching process of the shape memory programming cycle is enough to recover the network back to its initial state.

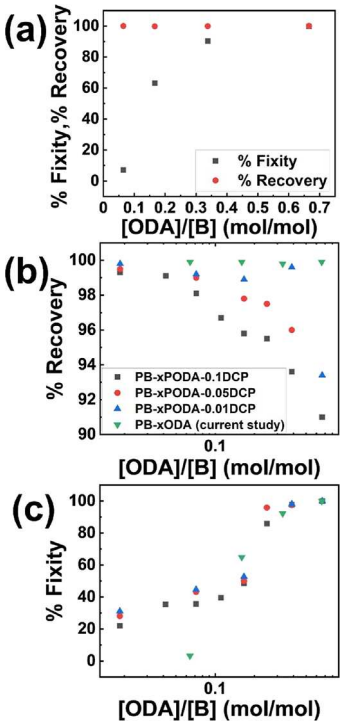

Figure 11. (a) Variation of % recovery and % fixity vs [ODA]/[B] from the 2nd programming cycle of the stress-controlled SMP cycles; (b, c) % recovery (b) and % fixity (c) (symbols listed in the legend in panel (b)) of annealed PB-*x*PODA-*y*DCP samples (cured with 0.1, 0.05, and 0.01 wt % DCP) and annealed PB-*x*ODA (thermally annealed samples). While PB-*x*PODA-*y*DCP samples were programmed at 60 °C, fixed at 20 °C, and recovered at 60 °C, PB-*x*ODA samples were programmed at 70 °C, fixed at 20 °C, and recovered at 70 °C. % fixity and % recovery data for PB-*x*PODA-*y*DCP samples (cured with 0.1, 0.05, and 0.01 wt % DCP) are reproduced with permission from ref 18. Copyright 2022, published by Wiley-VCH GmbH.

Figure 11b,c compares the shape memory properties of annealed PB-*x*ODA (current study) and annealed PB-*x*PODA-*y*DCP samples (previous study using peroxide curing and using PB with a different molecular weight and higher 1,2 content[18]). While a plateau is observed in the fixity at high ODA loading in the peroxide cured samples, a more continuous decrease is observed in annealed PB-*x*ODA. This plateau was attributed to the formation of a highly percolated network of PODA crystals, forming a rigid solid phase able to withstand the elastic restoring force of the stretched elastomer. In the case of the thermally annealed sample, a more continuous decrease in the fixity is observed. This is likely due to the differences in the morphologies of the sample. In the case of the annealed PB-*x*PODA-*y*DCP, the degree of crystallinity of the PODA matched that of pure PODA at equivalent loading, while in the annealed PB-*x*ODA, the degree of crystallinity as inferred from the DSC results in Figure 6c drops significantly compared to pure PODA with decreased ODA loading. Therefore, higher loadings of ODA are required to generate a structure-spanning network to fix the deformed sample compared to in situ-polymerized PODA. The results in Figure11a are plotted vs ODA weight fraction in Figure S8 in the Supporting Information. High % fixity and % recovery of ca. 100% are obtained at 80% ODA loading. Compared to other cross-linked elastomer/in situ-polymerized PODA systems, similar fixity is achieved at 70 wt % ODA (PB-*x*PODA-*y*DCP),[18] 70 wt % ODA (natural rubber/PODA),[21] and 60 wt % ODA (butyl rubber/PODA).[20]

The recovery behavior between the two systems also shows a marked difference. In the peroxide cured samples, the higher fixity resulted in a lower recovery. This was attributed to the presence of uncross-linked PB in the sample, which could stress-relax in the fixed sample, lowering the recovery. However, in the present study, since the sol fraction comprises entirely ODA at these ODA loadings (Figure S2), there is minimal uncross-linked PB limiting the extent of stress relaxation, resulting in a ∼100% recovery over the range of ODA loading. This was confirmed by comparing stress-relaxation measurements on the annealed PB-*x*ODA and annealed PB-*x*PODA-*y*DCP samples (y is the wt % of the DCP relative to the total weight of the polymer), where the samples with low extents of stress relaxation display high recovery (Figure S9, Supporting Information).

The annealed PB-*x*ODA samples with high ODA loading are potentially useful as easily fabricated shape memory polymers

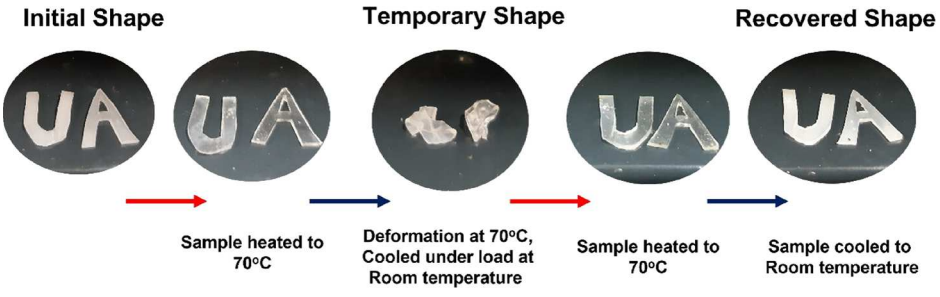

Figure 12. Shape memory demonstration of annealed PB-0.66ODA-M molded into a sheet (fixed at RT and recovered at 70 °C).

https://doi.org/10.1021/acsapm.3c00319
ACS Appl. Polym. Mater. XXXX, XXX, XXX−XXX

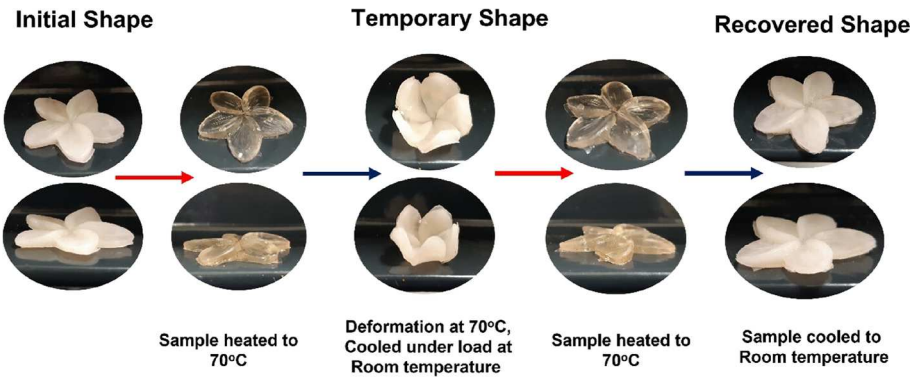

Figure 13. Shape memory demonstration of annealed PB-0.66ODA-M molded in the shape of a flower (fixed at RT and recovered at 70 °C).

that can be programmed without any cryogenic cooling. PB-0.66ODA was chosen as the model material to demonstrate the potential of this material to compound a shape memory polymer through melt mixing and curing. The initial high content of ODA (80 wt % ODA) allows the ODA to be used as a solvent to dissolve the PB and the solution was poured into a sheet mold (Figure 12) and a flower mold (Figure 13).

The gel fraction (G) and the swelling ratio (SR) of annealed PB-0.66ODA-M were found to be 0.701 and 10.2, compared to 0.700 and 10.1 in the case of annealed PB-0.66ODA, respectively. The similarity in the network properties proves that the samples processed via melt mixing and solvent mixing are alike, and thus, the mixed melt samples are expected to show similar shape memory properties to the solvent mixed samples.

Figures 12 and 13 show the macroscopic shape memory cycle of annealed PB-0.66ODA for both film samples from a sheet mold (Figure 12) and a more complex flower mold (Figure 13). Time lapse images of the recovery of the sample from the flower mold are shown in the Supporting Information (Figure S10), demonstrating that shape recovery at 70 °C occurs in about 80 s.

To isolate the effect of the mixture of grafted ODA and free ODA on the shape memory properties of annealed PB-xODA, control experiments were run with blends of PB and n-eicosane (PB-xEI). The DSC heating curves of these annealed PB-xEI samples are shown in Figure S11a (Supporting Information), and they have peak melting temperatures of 39−40 °C, similar to the annealed PB-xODA. Figure S11b (Supporting Information) shows the shape memory properties of annealed PB-xEI and annealed PB-xODA samples (quantitative values are listed in Table S7, Supporting Information), which show similar variation of % fixity and % recovery vs ODA or EI weight fraction.

A clear difference in the annealed PB-xODA and annealed PB-xEI is observed in the aging and repeated cycling of the samples. Figure 14 shows the shape memory properties and the weight of the recovered sample of annealed PB-0.66ODA and annealed PB-0.76EI over 10 cycles (Table S8, Supporting Information lists the data). The % fixity and % recovery of annealed PB-0.66ODA (with 80 wt % ODA) samples show minimal loss with a decrease in % fixity of 0.4%, a decrease % recovery of 0.3%, and a weight loss of 0.65% over 10 cycles. The annealed PB-0.76EI (80 wt % EI) samples exhibit a decrease in % fixity of 1.4%, decrease in % recovery of 0.2%, and weight loss of 4% over 10 cycles. The reduction in the fixity is attributed to the loss of the crystalline EI during

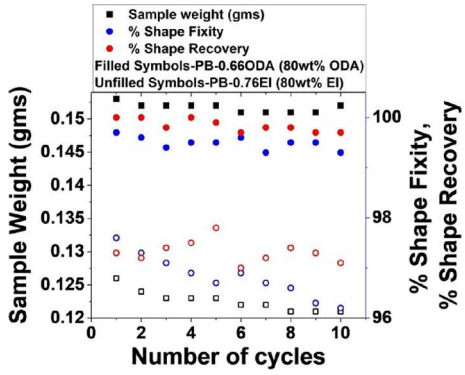

Figure 14. Shape memory properties and the sample weight (g) of the recovered semi crystalline annealed PB-0.66ODA (80 wt % ODA) and annealed PB-0.76EI (80 wt % EI) after each shape memory cycle.

cycling. While Figure 15a shows the aging of the annealed PB-0.66ODA under an ambient atmosphere, it reveals no observable blooming even after 85 days of aging. Figure 15b shows the aging of the annealed PB-0.76EI under an ambient atmosphere, and it reveals blooming after 15 days of aging, which worsens after 50 days. Blooming has been an issue in blends of a cross-linked elastomer with a crystalline small molecule likely due to the elastic restoring force driving melting, diffusion, and surface recrystallization, especially samples prepared by swelling.[15,16] Grafting ODA onto the PB chains results in connectivity between the elastomer (PB) and the small molecule (ODA) resisting blooming similar to the case of sulfonated EPDM and neutralized fatty acids.[17]

4. CONCLUSIONS

The high-temperature thermal annealing of blends of high *cis*-1,4-polybutadiene (PB) and octadecyl acrylate (ODA) results in a combination of PB cross-linking and ODA grafting to the PB to produce materials with shape memory behavior. At high ODA loading (e.g., 80 wt %), materials with excellent shape memory properties are obtained. The notable properties of these materials are the following: first, they can be prepared by melt-compounding and processing without the use of any added cross-linking agents, such as peroxides; second, the high incorporation of PB into the cross-linking network (i.e., high gel fraction) results in networks that exhibit low stress relaxation that translates into high shape recovery during shape memory cycling; third, the incomplete grafting of the ODA is not deleterious to the material stability, as the grafted units appear to compatibilize the PB and free ODA, limiting

https://doi.org/10.1021/acsapm.3c00319
ACS Appl. Polym. Mater. XXXX, XXX, XXX−XXX

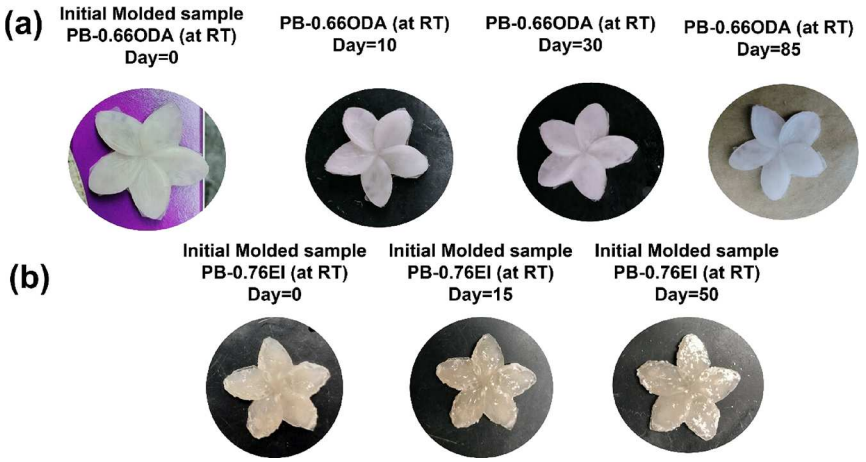

Figure 15. (a) Aging of annealed PB-0.66ODA (PB loaded with 80 wt % ODA) and (b) aging of annealed PB-0.76EI (PB loaded with 80 wt % EI).

the blooming and expulsion of the free ODA during storage and shape memory cycling. For practical use, materials containing unreacted acrylates are not desirable due to their potential as environmental and health hazards and therefore would need to be extracted, reacted to complete conversion, or replaced with more reactive enophiles, such as maleimides or triazolinediones. More generally, this fabrication route should be useful to incorporate other functionalities besides side-chain crystallinity, such as hydrophilicity. In addition, the cross-linking and grafting may be tolerant of functional groups and other compounds to allow the addition of a broad array of stimuli-responsive additives to tune the responsive properties of these materials.

■ ASSOCIATED CONTENT

Supporting Information

The Supporting Information is available free of charge at https://pubs.acs.org/doi/10.1021/acsapm.3c00319.

FTIR spectra (Figure S1), NMR spectra (Figure S2) and SEC traces of sol fractions (Figure S3), FTIR spectra and analysis of PB cross-linking (Figure S4), DSC traces of annealed and unannealed PB-*x*ODA (Figure S5), 2D WAXS images and WAXS peak analysis (Figure S6), DMA plots of shape memory tests (Figure S7), shape memory properties of annealed PB-*x*ODA samples (Figure S8), stress relaxation measurements (Figure S9), time-lapse images of shape recovery (Figure S10), shape memory properties of annealed PB-xEI samples (Figure S11), table of integral values of ODA sol fraction (Table S1), table of network properties (Table S2), tables of DSC data (Table S3 and S4), mechanical properties (Table S5 and S6), and shape memory properties (Table S7 and S8), derivation of conversion of c^* from g/cm^3 to ODA:PB repeat unit molar ratio (Appendix 1) (PDF)

■ AUTHOR INFORMATION

Corresponding Author

Kevin A. Cavicchi − *School of Polymer Science and Polymer Engineering, University of Akron, Akron, Ohio 44325-0301, United States;* orcid.org/0000-0002-6267-7899; Email: kac58@uakron.edu

Authors

Sayan Basak − *School of Polymer Science and Polymer Engineering, University of Akron, Akron, Ohio 44325-0301, United States*

Juan Camilo Marin Angel − *School of Polymer Science and Polymer Engineering, University of Akron, Akron, Ohio 44325-0301, United States;* Present Address: Avient Corporation, Avon Lake, Ohio 44012, United States. (J.C.M.A.)

Complete contact information is available at: https://pubs.acs.org/10.1021/acsapm.3c00319

Author Contributions

S.B.: conceptualization, methodology, investigation, writing-original draft, review & editing; J.C.M.A.: conceptualization, methodology; K.C.: conceptualization, writing-review & editing, supervision, project administration, funding acquisition.

Notes

The authors declare no competing financial interest.

■ ACKNOWLEDGMENTS

Financial support for S.B. from the NASA Glenn Research Center is acknowledged. This material is based on research sponsored by Air Force Research Lab under agreement number FA8650-20-2-1136. The U.S. Government is authorized to reproduce and distribute reprints for Governmental purposes notwithstanding any copyright notation thereon. The views and conclusions contained herein are those of the authors and should not be interpreted as necessarily representing the official policies or endorsements, either expressed or implied, of Air Force Research Lab or the U.S. Government. The authors acknowledge access to the X-ray scattering facility at the Advanced Materials and Liquid Crystal Institute (AMLCI) at Kent State University, which was financially supported by the National Science Foundation (DMR-2017845), the State of Ohio (The Ohio Department of Higher Education Action Fund), and Kent State University. The authors also thank Dr. Marianne Prévôt for her assistance in running the XRD instrument. The authors thank Dr. Tzu Yu Lai for her input in understanding the ene chemistry.

https://doi.org/10.1021/acsapm.3c00319
ACS Appl. Polym. Mater. XXXX, XXX, XXX−XXX

ABBREVIATIONS

SMP, shape memory polymers; ODA, octadecyl acrylate; PB, polybutadiene; PODA, polyoctadecyl acrylate; DPD, *N*,*N*′-diphenyl-*p*-phenylenediamine; AA, acetylacetone; GPC, gel permeation chromatography; ATR-FTIR, attenuated total reflection Fourier transform infrared; DMA, dynamic mechanical analyzer; *G*, gel Fraction; SR, swelling ratio; THF, tetrahydrofuran; RT, room temperature; DCP, dicumyl peroxide; EI, *n*-eicosane

REFERENCES

(1) Liang, C.; Rogers, C. A.; Malafeew, E. Investigation of Shape Memory Polymers and Their Hybrid Composites. *J. Intell. Mater. Syst. Struct.* **1997**, *8*, 380−386.

(2) Behl, M.; Razzaq, M. Y.; Lendlein, A. Multifunctional Shape-Memory Polymers. *Adv. Mater.* **2010**, *22*, 3388−3410.

(3) Hu, J.; Zhu, Y.; Huang, H.; Lu, J. Recent Advances in Shape−Memory Polymers: Structure, Mechanism, Functionality, Modeling and Applications. *Prog. Polym. Sci.* **2012**, *37*, 1720−1763.

(4) Zhang, J.; Yin, Z.; Ren, L.; Liu, Q.; Ren, L.; Yang, X.; Zhou, X. Advances in 4D Printed Shape Memory Polymers: From 3D Printing, Smart Excitation, and Response to Applications. *Adv Mater. Technol.* **2022**, *7*, 2101568.

(5) Morshedian, J.; Khonakdar, H. A.; Mehrabzadeh, M.; Eslami, H. Preparation and Properties of Heat-Shrinkable Cross-Linked Low-Density Polyethylene. *Adv. Polym. Technol.* **2003**, *22*, 112−119.

(6) Vernon, L. B.; Vernon, H. M. Process of manufacturing articles of thermoplastic synthetic resins. *U.S. Patent No.* 2,234,993. U.S. Patent and Trademark Office. Washington, DC, 1941 (Accessed 2023−02 -06).

(7) Manion, M. K. U.S. Patent Application No. 15/064,388, 2017. (Accessed 2023−02 -06).

(8) Delaey, J.; Dubruel, P.; Van Vlierberghe, S. Shape-Memory Polymers for Biomedical Applications. *Adv. Funct. Mater.* **2020**, *30*, 1909047.

(9) Li, X.; Wang, L.; Li, Y.; Xu, S. Reprocessable, Self-Healing, Thermadapt Shape Memory Polycaprolactone via Robust Ester−Ester Interchanges toward Kirigami-Tailored 4D Medical Devices. *ACS Appl. Polym. Mater.* **2023**, 1585.

(10) Takahashi, T.; Hayashi, N.; Hayashi, S. Structure and Properties of Shape-Memory Polyurethane Block Copolymers. *J. Appl. Polym. Sci.* **1996**, *60*, 1061−1069.

(11) Cavicchi, K. A. Shape Memory Polymers from Blends of Elastomers and Small Molecule Additives. *Macromol. Symp.* **2015**, *358*, 194−201.

(12) Zhang, Q.; Hua, W.; Feng, J. A Facile Strategy to Fabricate Multishape Memory Polymers with Controllable Mechanical Properties. *Macromol. Rapid Commun.* **2016**, *37*, 1262−1267.

(13) Brostowitz, N. R.; Weiss, R. A.; Cavicchi, K. A. Facile Fabrication of a Shape Memory Polymer by Swelling Cross-Linked Natural Rubber with Stearic Acid. *ACS Macro Lett.* **2014**, *3*, 374−377.

(14) Zhao, X.-Y.; Lu, Y.-L.; Xiao, D.-L.; Wu, S.-Z.; Zhang, L.-Q. Thermoplastic Ternary Hybrids of Polyurethane, Hindered Phenol and Hindered Amine with Selective Two-Phase Dispersion. *Macromol. Mater. Eng.* **2009**, *294*, 345−351.

(15) Winters, I. D. The rheological and structural properties of blends of polyethylene with paraffin wax, PhD Thesis, Georgia Institute of Technology, 2012.

(16) Pantoja, M.; Lin, Z.; Cakmak, M.; Cavicchi, K. A. Structure-Property Relationships of Fatty Acid Swollen, Crosslinked Natural Rubber Shape Memory Polymers. *J. Polym. Sci., Part B: Polym. Phys.* **2018**, *56*, 673−688.

(17) Dong, J.; Weiss, R. A. Shape Memory Behavior of Zinc Oleate-Filled Elastomeric Ionomers. *Macromolecules* **2011**, *44*, 8871−8879.

(18) Basak, S.; Cavicchi, K. A. Structure−Property Relationships of Shape Memory, Semicrystalline Polymers Fabricated by In Situ Polymerization and Crosslinking of Octadecyl Acrylate/Polybutadiene Blends. *Macromol. Rapid Commun.* **2023**, *44*, 2200404.

(19) Du, H.; Marin Angel, J.; Basak, S.; Lai, T.; Cavicchi, K. A. Cross-Linked Poly(Octadecyl Acrylate)/Polybutadiene Shape Memory Polymer Blends Prepared by Simultaneous Free Radical Cross-Linking, Grafting and Polymerization of Octadecyl Acrylate/Polybutadiene Blends. *Macromol. Rapid Commun.* **2021**, *42*, 2100072.

(20) Su, E.; Bayazit, G.; Ide, S.; Okay, O. Butyl Rubber-Based Interpenetrating Polymer Networks with Side Chain Crystallinity: Self-Healing and Shape-Memory Polymers with Tunable Thermal and Mechanical Properties. *Eur. Polym. J.* **2022**, *168*, No. 111098.

(21) Akca, O.; Okay, O. Shape-Memory Semicrystalline Polymeric Materials Based on Various Rubbers. *Macromol. Mater. Eng.* **2022**, *307*, 2100776.

(22) Su, E.; Bilici, C.; Bayazit, G.; Ide, S.; Okay, O. Solvent-Free UV Polymerization of N-Octadecyl Acrylate in Butyl Rubber: A Simple Way to Produce Tough and Smart Polymeric Materials at Ambient Temperature. *ACS Appl. Mater. Interfaces* **2021**, *13*, 21786−21799.

(23) Luchtenberg, J.; Ritter, H. Synthesis of Crystallizable Comb-like Oligomers by Coupling of Stearyl Acrylate to Butadiene Oligomers via Ene Reaction and the Influence of Side-Chain Order on the Network Formation by Autoxidation. *Macromol. Chem. Phys.* **1994**, *195*, 1623−1632.

(24) Sadeghi, G. M. M.; Afshar, T. F.; Morshedian, J.; Barikani, M. Determination of microstructure of back-bone of the polybutadiene-OL by FTIR and NMR spectroscopy. *Iranian Polymer Journal* **2003**, 515.

(25) Luchtenberg, J.; Ritter, H. Synthesis of photopolymerizable oligomers by coupling of 2-methacryloyloxyethyl acrylate via selective ene-reaction to oligobutadienes. *Macromol. Rapid Commun.* **1994**, *15*, 81−86.

(26) Binder, J. L. The Infrared Spectra and Structures of Polybutadienes. *J. Polym. Sci., Part A: Gen. Pap.* **1963**, *1*, 47−58.

(27) Jian, Y.; He, Y.; Wang, J.; Yang, W.; Nie, J. Rapid Solid-State Photopolymerization of Octadecyl Acrylate: Low Shrinkage and Insensitivity to Oxygen. *Polym. Int.* **2013**, *62*, 1692−1697.

(28) Wang, W.; Hutchinson, R. A. Free-Radical Acrylic Polymerization Kinetics at Elevated Temperatures. *Chem. Eng. Technol.* **2010**, *33*, 1745−1753.

(29) Riazi, H.; Shamsabadi, A. A.; Corcoran, P.; Grady, M. C.; Rappe, A. M.; Soroush, M. On the thermal self-initiation reaction of n-butyl acrylate in free-radical polymerization. *Processes* **2018**, *6*, 3.

(30) Flory, P. J. The mechanism of vinyl polymerizations1. *J. Am. Chem. Soc.* **1937**, *59*, 241−253.

(31) Yao, M.; Nie, J.; He, Y. Can chain-reaction polymerization of octadecyl acrylate occur in crystal? *Macromolecules* **2018**, *51*, 3731−3737.

(32) Jordan, E. F., Jr.; Feldeisen, D. W.; Wrigley, A. N. Side-chain crystallinity. . Heats of fusion and melting transitions on selected homopolymers having long side chains. I. *J. Polym. Sci., Part A-1: Polym. Chem.* **1971**, *9*, 1835−1851.

(33) Grassie, N.; Heaney, A. Thermal Reaction of Pendent Vinyl Groups in Polybutadiene and Copolymers of Butadiene and Acrylonitrile. *J. Polym. Sci., Polym. Lett. Ed.* **1974**, *12*, 89−94.

(34) Golub, M. A.; Sung, M. Thermal cyclization of 1,2-polybutadiene and 3,4-polyisoprene. *J. Polym. Sci., Polym. Lett. Ed.* **1973**, *11*, 129−138.

(35) Golub, M. A. Thermal Rearrangements of Polybutadienes with Different Vinyl Contents. *J. Polym. Sci., Polym. Chem. Ed.* **1981**, *19*, 1073−1083.

(36) Doskočilová, D.; Straka, J.; Schneider, B. Study of Thermal Degradation of Polybutadiene in Inert Atmosphere: 2. Characterization of Thermal Crosslinking in Polybutadiene by High Resolution Solid State 13C and 1H Magic Angle Spinning N.m.r. Spectroscopy. *Polymer* **1993**, *34*, 437−439.

(37) Ziaee, F.; Mobarakeh, H. S.; Nekoomanesh, M. Thermal Rearrangement Study of Low Molecular Weight Polybutadiene. *Polym. Degrad. Stab.* **2009**, *94*, 1336−1343.

https://doi.org/10.1021/acsapm.3c00319
ACS Appl. Polym. Mater. XXXX, XXX, XXX−XXX

(38) Ziaee, F.; Mobarakeh, H. S.; Nekoomanesh, M.; Arabi, H. Study of Tacticity and Thermal Rearrangement of Low Molecular Weight 1,2- Polybutadiene by NMR. *e-Polymers* **2008**, *8* (), DOI: 10.1515/epoly.2008.8.1.1357.
(39) Ronagh-Baghbani, M.; Ziaee, F.; Bouhendi, H.; Ziaie, F. Crosslinking Investigation of Polybutadiene Thermal Degradation by Carbon-13 Nuclear Magnetic Resonance. *Polym. Degrad. Stab.* **2011**, *96*, 1805−1811.
(40) Hoffmann, H. M. R. The Ene Reaction. *Angew. Chem., Int. Ed.* **1969**, *8*, 556−577.
(41) Sunday, D. F.; Chremos, A.; Martin, T. B.; Chang, A. B.; Burns, A. B.; Grubbs, R. H. Concentration Dependence of the Size and Symmetry of a Bottlebrush Polymer in a Good Solvent. *Macromolecules* **2020**, *53*, 7132−7140.
(42) Graessley, W. Polymer Chain Dimensions and the Dependence of Viscoelastic Properties on Concentration, Molecular Weight and Solvent Power. *Polymer* **1980**, *21*, 258−262.
(43) Makhiyanov, N.; Davletbaev, R. R. Kuhn−Mark−Houwink−Sakurada Coefficients for Determination of Molecular Parameters of Cis-Polybutadiene Rubbers by Gel Permeation Chromatography. *Polym. Sci., Ser. A* **2018**, *60*, 117−126.
(44) Boborodea, A.; O'Donohue, S. Universal Calibration of Gel Permeation Chromatography Using Evaporative Light Scattering Detector Coupled with Viscometer. *Int. J. Polym. Anal. Charact.* **2020**, *25*, 167−175.
(45) Hiemenz, P. C.; Lodge, T. P. Polymer Chemistry. *CRC Press* **2007**, DOI: 10.1201/9781420018271.
(46) Spychal, T.; Lath, D.; Berek, D. Thermodynamic and Hydrodynamic Properties of the the Systems Polymer—Tetrahydrofuran—Water: 1 Solution Properties of Polystyrene. *Polymer* **1979**, *20*, 437−442.
(47) Garraza, A. R.; Sorichetti, P.; Marzocca, A. J.; Matteo, C. L.; Monti, G. A. Influence of the microstructure of vulcanized polybutadiene rubber on the dielectric properties. *Polym. Test.* **2011**, *30*, 657−662.
(48) Leyrer, R. J.; Mächtle, W. Emulsion polymerization of hydrophobic monomers like stearyl acrylate with cyclodextrin as a phase transfer agent. *Macromol. Chem. Phys.* **2000**, *201*, 1235−1243.
(49) Inomata, K.; Sakamaki, Y.; Nose, T.; Sasaki, S. Solid-State Structure of Comb-like Polymers Having N-Octadecyl Side Chains I. Cocrystallization of Side Chain with N-Octadecanoic Acid. *Polym. J.* **1996**, *28*, 986−991.
(50) Saikia, P. J.; Baruah, S. D. Structural and Thermal Behavior of Comb-like Polymer Havingn-Octadecyl Side Chains. *J. Appl. Polym. Sci.* **2007**, *104*, 1226−1231.
(51) Rubin, I. D.; Pugliese, R. D. *Angew. Makromol. Chem.* **1989**, *171*, 165−173.
(52) Platé, N. A.; Shibaev, V. P. Comb-like Polymers. Structure and Properties. Journal of Polymer Science. *Macromol. Rev.* **1974**, *8*, 117−253.
(53) Hsieh, H. W. S.; Post, B.; Morawetz, H. A Crystallographic Study of Polymers Exhibiting Side-Chain Crystallization. *J. Polym. Sci., Polym. Phys. Ed.* **1976**, *14*, 1241−1255.
(54) Xiang, M.-Y.; Lyu, D.; Liu, L.-Z.; Men, Y.-F. Limited Fraction of Crystallized Side Chains in Bottlebrush Poly(N-Alkyl Methacrylate)S. *Chin. J. Polym. Sci.* **2021**, *39*, 1211−1216.
(55) Jordan, E. F.; Smith, S.; Zabarsky, R. D.; Wrigley, A. N. Viscosity Index. III. Thermodynamic Parameters for Side Chain Crystallinity in Pour Point-Modified Blends Containing N-Octadecyl Acrylate. *J. Appl. Polym. Sci.* **1978**, *22*, 1547−1567.
(56) Jordan, E. F.; Side-Chain Crystallinity, V. Heats of Fusion and Melting Temperatures on Monomers Whose Homopolymers Have Long Side Chains. Journal of Polymer Science Part A-1. *Polym. Chem.* **1972**, *10*, 3347−3366.
(57) Mooney, M. A theory of large elastic deformation. *J. Appl. Phys.* **1940**, *11*, 582−592.
(58) Rivlin, R. Large elastic deformations of isotropic materials. I. Fundamental concepts. *Philos. Trans. Royal Soc. A* **1948**, *240*, 459−490.
(59) Gula, I. A.; Karimi-Varzaneh, H. A.; Svaneborg, C. Computational Study of Cross-Link and Entanglement Contributions to the Elastic Properties of Model PDMS Networks. *Macromolecules* **2020**, *53*, 6907−6927.
(60) Syed, I. H.; Stratmann, P.; Hempel, G.; Klüppel, M.; Saalwächter, K. Entanglements, Defects, and Inhomogeneities in Nitrile Butadiene Rubbers: Macroscopic versus Microscopic Properties. *Macromolecules* **2016**, *49*, 9004−9016.
(61) Boyer, R. F.; Miller, R. L. Correlations Involving the Mooney—Rivlin C2 Constant and the Number of Chain Atoms between Physical Entanglements. *Nc. Polymer* **1987**, *28*, 399−407.
(62) Lin, D. C.; Douglas, J. F.; Horkay, F. Development of Minimal Models of the Elastic Properties of Flexible and Stiff Polymer Networks with Permanent and Thermoreversible Cross-Links. *Soft Matter* **2010**, *6*, 3548−3561.
(63) Douglas, J. F. Influence of Chain Structure and Swelling on the Elasticity of Rubbery Materials: Localization Model Description. *Macromol. Symp.* **2013**, *329*, 87−100.
(64) Sombatsompop, N. Practical use of the Mooney-Rivlin equation for determination of degree of crosslinking of swollen nr vulcanisates. *J. Sci. Soc. Thai.* **1988**, *24*, 199−204.
(65) Gaylord, R. J.; Douglas, J. F. Rubber Elasticity: A Scaling Approach. *Polym. Bull.* **1987**, *18*, 347.
(66) Blokland, R.; Prins, W. Elasticity and Structure of Chemically Crosslinked Polyurethanes. Journal of Polymer Science Part A-2: Polymer. *Physics* **1969**, *7*, 1595−1618.
(67) Schlögl, S.; Trutschel, M.-L.; Chassé, W.; Riess, G.; Saalwächter, K. Entanglement Effects in Elastomers: Macroscopic vs Microscopic Properties. *Macromolecules* **2014**, *47*, 2759−2773.
(68) Halasa, A. F.; Wathen, G. D.; Hsu, W. L.; Matrana, B. A.; Massie, J. M. Relationship between interchain spacing of amorphous polymers and blend miscibility as determined by wide-angle X-ray scattering. *J. Appl. Polym. Sci.* **1991**, *43*, 183−190.
(69) Inomata, K.; Sakamaki, Y.; Nose, T.; Sasaki, S. Solid-state structure of comb-like polymers having n-octadecyl side chains II. Crystalline-amorphous layered structure. *Polym. J.* **1996**, *28*, 992−999.
(70) Xiang, M.; Lyu, D.; Qin, Y.; Chen, R.; Liu, L.; Men, Y. Microstructure of bottlebrush poly (n-alkyl methacrylate) s beyond side chain packing. *Polymer* **2020**, *210*, No. 123034.
(71) Fetters, L. J.; Lohse, D. J.; Richter, D.; Witten, T. A.; Zirkel, A. Connection between Polymer Molecular Weight, Density, Chain Dimensions, and Melt Viscoelastic Properties. *Macromolecules* **1994**, *27*, 4639−4647.

https://doi.org/10.1021/acsapm.3c00319
ACS Appl. Polym. Mater. XXXX, XXX, XXX−XXX